

TURBULENT ENERGY SPECTRUM VIA AN INTERACTION POTENTIAL

RAFAIL V. ABRAMOV

ABSTRACT. For a large system of identical particles interacting by means of a potential, we find that a strong large scale flow velocity can induce motions in the inertial range via the potential coupling. This forcing lies in special bundles in the Fourier space, which are formed by pairs of particles. These bundles are not present in the Boltzmann, Euler and Navier–Stokes equations, because they are destroyed by the Bogoliubov–Born–Green–Kirkwood–Yvon formalism. However, measurements of the flow can detect certain bulk effects shared across these bundles, such as the power scaling of the kinetic energy. We estimate the scaling effects produced by two types of potentials: the Thomas–Fermi interatomic potential (as well as its variations, such as the Ziegler–Biersack–Littmark potential), and the electrostatic potential. In the near-viscous inertial range, our estimates yield the inverse five-thirds power decay of the kinetic energy for both the Thomas–Fermi and electrostatic potentials. The electrostatic potential is also predicted to produce the inverse cubic power scaling of the kinetic energy at large inertial scales. Standard laboratory experiments confirm the scaling estimates for both the Thomas–Fermi and electrostatic potentials at near-viscous scales. Surprisingly, the observed kinetic energy spectrum in the Earth atmosphere at large scales behaves as if induced by the electrostatic potential. Given that the Earth atmosphere is not electrostatically neutral, we cautiously suggest a hypothesis that the atmospheric kinetic energy spectra in the inertial range are indeed driven by the large scale flow via the electrostatic potential coupling.

1. INTRODUCTION

The phenomenon of turbulence in fluids has first been documented by Leonardo da Vinci, and later by Boussinesq [5] and Reynolds [32,33]. As observed, turbulent motions in fluids appear to be caused by the presence of a strong large scale flow, and manifest in the ranges between the large and viscous scales (the so-called “inertial range”). In 1941, Kolmogorov [22–24] suggested that the power scaling of the turbulent kinetic energy spectrum could be modeled via an *ad hoc* dimensional hypothesis. With help of Kolmogorov’s hypothesis, Obukhov [28,29], Chandrasekhar [10], Corrsin [12], and others observed that the time-averaged kinetic energy spectrum in many real-world turbulent flows scales in the Fourier space as the inverse five-thirds power of the wavenumber (known as the “Kolmogorov spectrum”). Although various other hypotheses on the nature of the five-thirds spectrum have been proposed since then, none of those, to our knowledge, offer a definitive physical explanation of why such a spectrum manifests itself, relying instead upon additional *ad hoc* assumptions.

DEPARTMENT OF MATHEMATICS, STATISTICS AND COMPUTER SCIENCE, UNIVERSITY OF ILLINOIS AT CHICAGO, 851 S. MORGAN ST., CHICAGO, IL 60607

E-mail address: abramov@uic.edu.

Curiously, the major proposed hypotheses for the turbulent kinetic energy spectra have one feature in common – namely, they rely upon conventional models of fluid dynamics, such as the Euler or Navier–Stokes equations. In the current work, we consider a possibility that the main reason for this long standing difficulty with the description of turbulence is that the standard fluid dynamics equations lack the necessary physical effects to naturally recover turbulent features in a flow. In order to see why this might happen, here we start with reviewing the microscopic dynamics of fluid motion and the standard derivation of the Navier–Stokes and Euler equations from the kinetic model of a multiparticle fluid, and point out possible reasons for such a peculiar deficiency.

Within the scope of the classical mechanics, a fluid consists of many identical particles, each pair of which interact (mostly repel, but sometimes attract) via a potential. If the potential function is known, then one can explicitly formulate the system of first-order ordinary differential equations (ODE) for the coordinate and velocity of each particle as functions of time. Using the vector field of this system, one can also derive the first-order linear partial differential equation (PDE) for the probability density of states of this system, which is known as the Liouville [8,9,14], forward Kolmogorov [1,15,31], or Fokker–Planck [34] equation.

For a system of N particles, the Liouville equation is a $3N$ -dimensional PDE, and, of course, cannot be solved explicitly in real-world scenarios (where $N \sim 10^{23}$). For a practical computation, the following simplifications are made. First, it is assumed that the interaction potential has a very short range, so that its effect can be approximated via a “hard sphere collision” interaction [3,8,9,18]. Second, it is assumed that the probability density of the complete system is symmetric under the permutations of particles (that is, the particles behave statistically identically). This allows to use the Bogoliubov–Born–Green–Kirkwood–Yvon (BBGKY) formalism [2,4,20] to obtain a PDE for the marginal probability density of a single particle, which, however, depends on the joint two-particle distribution. Third, the additional assumption of statistical independence of all particles is used to express the two-particle probability distribution as a product of two single-particle distributions. The resulting standalone equation for the probability distribution of a single particle is known as the Boltzmann equation [3,8,9]. The effects of interactions between different particles are approximated by the collision integral of the Boltzmann equation.

To obtain the Euler or Navier–Stokes equations, the Boltzmann equation is further integrated against various powers of the velocity variable. The zero-order moment equation becomes the evolution equation for the density of the fluid, the first-order moment equation describes the velocity, while the contracted second-order moment equation is the one for the energy. Due to the mass, momentum and energy conservation laws, the corresponding velocity moments of the Boltzmann collision integral disappear from these three moment equations. Further, if the higher-order non-Gaussian moments of the solution are presumed to be zero, the compressible Euler equations emerge [17]. If however, the higher-order moments are parameterized from the equations for the stress and heat flux via the Chapman–Enskog expansion [11,19] and the resulting Newton and Fourier laws of viscosity and heat conductivity, respectively, then the compressible Navier–Stokes equations are obtained [18]. In many practical applications, the flows are

effectively incompressible, in which case the zero-order density moment is treated as a constant, leading to the incompressible Euler and Navier–Stokes equations.

As we can see, in order to arrive at the standard equations of fluid dynamics from the Liouville equation, one has to make some drastic simplifications, which are based on rather strong assumptions. In the present work, we entertain a hypothesis that the apparent lack of turbulent effects in conventional models of fluid mechanics is caused by these simplifications. To this end, we directly investigate the Liouville equation for N particles, which interact via a generic potential. What we uncover is that a strong large scale flow velocity creates forcing in the inertial scales via the potential. This forcing manifests in special 3-dimensional bundles of the full $3N$ -dimensional coordinate space, which are shared by all unordered pairs of particles. As suspected, these bundles are indeed destroyed in the course of the BBGKY formalism, so that no such forcing manifests in the Boltzmann equation, and, subsequently, in the Euler and Navier–Stokes equations. At the same time, it turns out that measurements can detect some bulk effects of the strong large scale flow forcing, if they are shared across these bundles.

Next, we estimate the scaling of suitably windowed time averages of solutions of the Liouville equation for N particles, which interact via either the Thomas–Fermi interatomic potential [13, 37] (and variations, such as the Ziegler–Biersack–Littmark potential [38]), or the electrostatic potential. Assuming that the inertial range motions are driven by a strong large scale flow velocity via a potential, for a suitable averaging time scale we find that:

- a. In a small scale turbulent flow (in the proximity of the viscous range), the time averages of the kinetic energy should scale as the inverse five-thirds power of the wavenumber for both the Thomas–Fermi and the electrostatic potentials;
- b. In a larger scale turbulent flow, the time averages of the kinetic energy should scale as the inverse cubic power of the wavenumber for the electrostatic potential. On the other hand, the Thomas–Fermi potential has a short effective range, and thus is not expected to affect the motion at large scales in any specific way.

An interesting observation is that the physical mechanism of creation of these energy spectra is absent from the conventional Euler and Navier–Stokes equations, since the latter do not contain the potential interaction terms in the energy equation.

To compare the theoretically predicted turbulent energy spectra with the observations, we refer to the works of Buchhave and Velte [6], and Nastrom and Gage [27]. In [6], the turbulent energy spectra are measured in laboratory conditions, and exhibit the scaling behavior consistent with the predictions for the Thomas–Fermi potential. In [27], the turbulent energy spectra are computed from direct observations of the atmospheric flow. Surprisingly, the decay of the turbulent energy spectra in [27] is more consistent with the electrostatic potential, since they have the evidence of both the inverse five-thirds power scaling at small scales, and the inverse cubic power scaling at larger scales. Given that the Earth atmosphere is not electrostatically neutral, we suggest a hypothesis that the atmospheric turbulent energy spectra could indeed be produced by the large scale flow coupled to the inertial ranges via the electrostatic potential.

2. A SYSTEM OF INTERACTING PARTICLES AND ITS LIOUVILLE EQUATION

We start with a system of N identical particles, which interact via a potential $\phi(r)$. Here, any given particle, situated at the coordinate point \mathbf{y} , creates the potential field $\phi(\|\mathbf{x} - \mathbf{y}\|)$ around itself. Subsequently, any other particle, placed at the point \mathbf{x} , experiences the acceleration given via

$$(2.1) \quad \mathbf{a} = -\frac{\partial}{\partial \mathbf{x}} \phi(\|\mathbf{x} - \mathbf{y}\|).$$

The total acceleration, experienced by an i -th particle, is thus given as the sum of contributions from the remaining particles:

$$(2.2) \quad \mathbf{a}_i = -\sum_{\substack{j=1 \\ j \neq i}}^N \frac{\partial}{\partial \mathbf{x}_i} \phi(\|\mathbf{x}_i - \mathbf{x}_j\|).$$

Above, \mathbf{x}_i and \mathbf{x}_j are the coordinate of i -th and j -th particles, respectively.

Knowing the accelerations, we can construct the system of equations of motion for the complete system of N particles as

$$(2.3) \quad \frac{d\mathbf{x}_i}{dt} = \mathbf{v}_i, \quad \frac{d\mathbf{v}_i}{dt} = \mathbf{a}_i = -\sum_{\substack{j=1 \\ j \neq i}}^N \frac{\partial}{\partial \mathbf{x}_i} \phi(\|\mathbf{x}_i - \mathbf{x}_j\|),$$

where \mathbf{v}_i is the velocity of the i -th particle. For further convenience, we concatenate $\mathbf{X} = (\mathbf{x}_1, \dots, \mathbf{x}_N)$, $\mathbf{V} = (\mathbf{v}_1, \dots, \mathbf{v}_N)$, and denote the combined potential via $\Phi(\mathbf{X})$:

$$(2.4) \quad \Phi(\mathbf{X}) = \sum_{i=1}^{N-1} \sum_{j=i+1}^N \phi(\|\mathbf{x}_i - \mathbf{x}_j\|).$$

Then, the system of equations of motion in (2.3) can be written in a vector form via

$$(2.5) \quad \frac{d}{dt} \begin{pmatrix} \mathbf{X} \\ \mathbf{V} \end{pmatrix} = \begin{pmatrix} \mathbf{V} \\ -\partial\Phi/\partial\mathbf{X} \end{pmatrix}.$$

Let $F(t, \mathbf{X}, \mathbf{V})$ be the probability distribution for the whole system of N particles, in the sense that, at time t , $F(t, \mathbf{X}, \mathbf{V})d\mathbf{X}d\mathbf{V}$ is the probability that the system can be found in the elementary phase volume $d\mathbf{X}d\mathbf{V}$ adjacent to the state (\mathbf{X}, \mathbf{V}) . Then, the corresponding Liouville [8,9,14] (also known as the forward Kolmogorov [1,15,31] or Fokker–Planck [34]) equation for F is given via

$$(2.6) \quad \frac{\partial F}{\partial t} + \mathbf{V} \cdot \frac{\partial F}{\partial \mathbf{X}} = \frac{\partial \Phi}{\partial \mathbf{X}} \cdot \frac{\partial F}{\partial \mathbf{V}}.$$

In what follows, it is convenient to transform the Liouville equation in a manner that removes the high-dimensional differentiation operators. We will use two different techniques for eliminating each of the operators – the moment integration for \mathbf{V} , and the Fourier transformation for \mathbf{X} .

2.1. The equations for velocity moments. To eliminate the V -derivative in the right-hand side of the Liouville equation (2.6), we integrate both sides of (2.6) against various powers of V , such that the V -derivative in the right-hand side of (2.6) can be removed via the integration by parts. This is a standard approach for the Boltzmann equation [3, 8], which leads to the conventional Euler equations [17]. We use the following standard notations for the velocity moments: the density ρ , average velocity vector \mathbf{U} , average kinetic energy matrix \mathbf{E} , and the cubic moment tensor \mathbf{M}_3 :

$$(2.7a) \quad \rho = \int_{\mathbb{R}^{3N}} F dV, \quad \rho \mathbf{U} = \int_{\mathbb{R}^{3N}} V F dV,$$

$$(2.7b) \quad \rho \mathbf{E} = \int_{\mathbb{R}^{3N}} V^2 F dV, \quad \rho \mathbf{M}_3 = \int_{\mathbb{R}^{3N}} V^3 F dV,$$

where by " V^k " we denote the outer product of k vectors. Integrating (2.6) against the outer powers of V above, and assuming that no surface integrals emerge, we arrive at

$$(2.8a) \quad \frac{\partial \rho}{\partial t} + \frac{\partial}{\partial X} \cdot (\rho \mathbf{U}) = 0, \quad \frac{\partial(\rho \mathbf{U})}{\partial t} + \frac{\partial}{\partial X} \cdot (\rho \mathbf{E}) = -\rho \frac{\partial \Phi}{\partial X},$$

$$(2.8b) \quad \frac{\partial(\rho \mathbf{E})}{\partial t} + \frac{\partial}{\partial X} \cdot (\rho \mathbf{M}_3) = -\rho \left(\frac{\partial \Phi}{\partial X} \mathbf{U}^T + \mathbf{U} \frac{\partial \Phi}{\partial X} \right).$$

In what is to follow, it is convenient to express the cubic moment \mathbf{M}_3 via the corresponding centered moment (or *skewness*). Namely, let us write the identity

$$(2.9) \quad V^3 = (V - U)^3 + U \otimes V \otimes V + V \otimes U \otimes V + V \otimes V \otimes U - \\ - V \otimes U \otimes U - U \otimes V \otimes U - U \otimes U \otimes V + U^3,$$

where " \otimes " denotes the outer product. Then, denote the skewness tensor \mathbf{Q} via the centered cubic moment

$$(2.10) \quad \rho \mathbf{Q} = \int_{\mathbb{R}^{3N}} (V - U)^3 F dV.$$

This allows to express the uncentered cubic moment \mathbf{M}_3 via

$$(2.11a) \quad \rho \mathbf{M}_3 = \int_{\mathbb{R}^{3N}} V^3 F dV = \rho(\mathbf{Q} + \mathbf{R}),$$

$$(2.11b) \quad \mathbf{R} = \mathbf{U} \otimes \mathbf{E} + (\mathbf{U} \otimes \mathbf{E})^T + (\mathbf{U} \otimes \mathbf{E})^{TT} - 2\mathbf{U}^3,$$

where " T " and " TT " denote the two cyclic permutations of the indices of a rank 3 tensor (which can be interpreted as two "transpositions", analogously to the single transposition of a matrix). The moment equations in (2.8) become

$$(2.12a) \quad \frac{\partial \rho}{\partial t} + \frac{\partial}{\partial X} \cdot (\rho \mathbf{U}) = 0, \quad \frac{\partial(\rho \mathbf{U})}{\partial t} + \frac{\partial}{\partial X} \cdot (\rho \mathbf{E}) = -\rho \frac{\partial \Phi}{\partial X},$$

$$(2.12b) \quad \frac{\partial(\rho \mathbf{E})}{\partial t} + \frac{\partial}{\partial X} \cdot (\rho(\mathbf{Q} + \mathbf{R})) = -\rho \left(\frac{\partial \Phi}{\partial X} \mathbf{U}^T + \mathbf{U} \frac{\partial \Phi}{\partial X} \right).$$

2.2. The Fourier transformation of the moment equations. To remove the X -derivative, the suitable technique is the Fourier transformation, since it replaces the differentiation operators with the wavevector multiplications. In what follows, we adopt the notation

$$(2.13) \quad \hat{i} = 2\pi\sqrt{-1},$$

to be able to use the letter “ i ” for indexing the summations below. Applying the Fourier transformation in X to (2.12), and denoting the wavevector as $\mathbf{K} = (k_1, \dots, k_N)$, we arrive at

$$(2.14a) \quad \frac{1}{\hat{i}} \frac{d\rho_K}{dt} + \mathbf{K} \cdot (\rho_K * \mathbf{U}_K) = 0, \quad \frac{1}{\hat{i}} \frac{d}{dt} (\rho_K * \mathbf{U}_K) + \mathbf{K} \cdot (\rho_K * \mathbf{E}_K) = -\rho_K * (\mathbf{K}\Phi_K),$$

$$(2.14b) \quad \frac{1}{\hat{i}} \frac{d}{dt} (\rho_K * \mathbf{E}_K) + \mathbf{K} \cdot (\rho_K * (\mathbf{Q}_K + \mathbf{R}_K)) = -\rho_K * \left[(\mathbf{K}\Phi_K) * \mathbf{U}_K^T + \mathbf{U}_K * (\mathbf{K}\Phi_K)^T \right],$$

where “ $*$ ” denotes the convolution in the Fourier space. The Fourier transform \mathbf{R}_K is given via

$$(2.15) \quad \mathbf{R}_K = \mathbf{U}_K \circledast \mathbf{E}_K + (\mathbf{U}_K \circledast \mathbf{E}_K)^T + (\mathbf{U}_K \circledast \mathbf{E}_K)^{TT} - 2\mathbf{U}_K \circledast \mathbf{U}_K \circledast \mathbf{U}_K,$$

where “ \circledast ” denotes the superposition of a convolution with an outer product.

3. POTENTIAL-INDUCED FORCING IN THE INERTIAL RANGE

What we obtained in (2.14) is an infinite-dimensional system of nonlinear ODE for the Fourier transforms ρ_K , \mathbf{U}_K and \mathbf{E}_K , with \mathbf{Q}_K being a set of “free parameters”. Obviously, this system has a broad range of formal solutions, and only a small subset of those is physically relevant. First, observe that, in the context of physics, the Fourier transform \mathbf{Q}_K of the skewness tensor in (2.10) is not a free parameter, but rather obeys its own set of equations, which involve even higher-order moments, and so forth (see the moment closure problem of molecular kinetics [11, 19, 26]). Second, even if we are somehow able to take all of those higher-order moments into account – which, effectively, amounts to solving the averaged Liouville equation in (2.6) – the latter will still have many solutions which are not physically relevant; for example, those where the particles are arranged in way so as to have a low-dimensional periodic motion, or even to avoid any interaction at all. Thus, in order to make meaningful conclusions from (2.14), we need to place qualitative restrictions on its solutions of interest, which correspond to a realistic behavior of the observed flow.

In practical scenarios, the typical observed structure of the system (say, the flow of a gas) consists of three distinct ranges of spatial scales:

- a. **The large scale flow.** Typically, there is a relatively small cluster of low-order Fourier wavenumbers, which contain a strong self-coupled solution describing the observed macroscopic phenomenon (for example, a jet or an eddy). This strong large-scale flow is typically “self-coupled”, in the sense that it can be accurately described by a reduced, simplified system which only couples together these large scale motions and excludes small-scale effects (for example, the stratified rotating Boussinesq, barotropic, or quasigeostrophic equations for Earth’s atmosphere). In what follows, we denote the Fourier transform of this strong large scale flow via

W_K (for convenience, we use a different letter for the strong large scale flow velocity to differentiate it from the “generic” inertial range velocity U_K).

- b. **The viscous range.** At the opposite side of the spectrum, on the scales of the average distance between the particles, the effect of the interaction potential ϕ becomes strong. As a result, the Fourier transform of the flow at small scales becomes nonlinearly coupled to itself via the interaction potential. The statistical macroscopic effect of this self-coupling is known as the *viscosity*, and can be derived in a standard fashion from the Boltzmann equation via the Chapman–Enskog expansion [1, 11, 18, 19]. The result is that the Fourier transform of the velocity decays exponentially rapidly in time at small scales, constituting an effective “cut-off” of the average velocity in the viscous range. To balance out the equations, this, in turn, triggers the growth of higher-order moments such as the skewness, the effects of which are observed in the form of the heat fluxes and the Fourier law of heat conductivity.
- c. **The inertial range.** The remaining range of the Fourier wavenumbers lies between the large scale flow and the viscous scales, and is known as the *inertial range*. On these scales, the effect of the interatomic potential ϕ is not strong enough to cause the effects of self-coupling, but, at the same time, it is still strong enough to induce motions via the coupling to the strong large-scale flow velocity W_K . This is the Fourier wavenumber range where the turbulent effects are observed.

In what follows, the wavenumber K in the moment equations (2.14) refers to the inertial range. In this range, we assume that the effect of the potential forcing can be completely neglected, with the exception of terms which are coupled to the large scale flow velocity W_K . This leads to the following simplification of (2.14) in the inertial range:

$$(3.1a) \quad \frac{1}{\hat{i}} \frac{d\rho_K}{dt} + K \cdot (\rho_K * U_K) = 0, \quad \frac{1}{\hat{i}} \frac{d}{dt} (\rho_K * U_K) + K \cdot (\rho_K * E_K) = 0,$$

$$(3.1b) \quad \frac{1}{\hat{i}} \frac{d}{dt} (\rho_K * E_K) + K \cdot (\rho_K * (Q_K + R_K)) = -\rho_K * \left[(K\Phi_K) * W_K^T + W_K * (K\Phi_K)^T \right].$$

Here, the Fourier transform W_K of the strong large scale flow velocity is treated as an “external forcing”, as we assume that the motions in the inertial range are weak enough to not cause any substantial feedback to the large scales via the potential. The corresponding damping is “hidden” in Q_K , and manifests as the Fourier law of heat conductivity at appropriate spatial and temporal scales.

Let us further assume that, at the initial time, the Fourier transforms ρ_K , U_K , E_K and Q_K in the inertial range are zero (that is, the flow is not turbulent initially). This means that any motions in the inertial range must be caused by the strong large scale flow velocity W_K via the potential coupling in the energy equation in (3.1). Thus, in order to understand how turbulent motions are produced in the inertial range, we need to examine the structure of the forcing induced via the strong large scale flow velocity W_K .

For the sake of simplicity of the argument, let us assume that the solution of (3.1) is nearly incompressible (which is indeed the case in many observed turbulent flows), and thus the Fourier transform ρ_K is largely restricted to its zero Fourier coefficient ρ_0 . For the energy equation, it means that the time derivative of the energy E_K , as well as the advection term $K \cdot (Q_K + R_K)$, are affected directly by the sum of the convolution

$(\mathbf{K}\Phi_{\mathbf{K}}) * \mathbf{W}_{\mathbf{K}}^T$ with its own transpose. In order to examine the structure of this convolution, let us write it directly via the integral:

$$(3.2) \quad (\mathbf{K}\Phi_{\mathbf{K}}) * \mathbf{W}_{\mathbf{K}}^T = \int_{\mathbb{R}^{3N}} (\mathbf{K} - \mathbf{K}') \Phi_{\mathbf{K}-\mathbf{K}'} \mathbf{W}_{\mathbf{K}'}^T d\mathbf{K}'.$$

To proceed, we need to know the structure of the Fourier transform $\Phi_{\mathbf{K}}$ of the combined potential. In Appendix A, we show in a straightforward fashion that $\Phi_{\mathbf{K}}$ has the form

$$(3.3) \quad \Phi_{\mathbf{K}} = \sum_{i=1}^{N-1} \sum_{j=i+1}^N \phi_{\|\mathbf{k}_i\|} \delta(\mathbf{k}_i + \mathbf{k}_j) \prod_{\substack{m=1 \\ m \neq i,j}}^N \delta(\mathbf{k}_m),$$

with $\phi_{\|\mathbf{k}\|}$ given via

$$(3.4) \quad \phi_{\|\mathbf{k}\|} = \frac{2}{\|\mathbf{k}\|} \int_0^\infty r \phi(r) \sin(2\pi \|\mathbf{k}\| r) dr.$$

Observe that the Fourier transform $\Phi_{\mathbf{K}}$ in (3.3) is zero for almost all $\mathbf{K} \in \mathbb{R}^{3N}$; in order for $\Phi_{\mathbf{K}}$ to be nonzero, \mathbf{K} must belong to a 3-dimensional subspace \mathcal{S}_{ij} of the form

$$(3.5) \quad \mathcal{S}_{ij} = \{\mathbf{K} = (\mathbf{0}, \dots, \mathbf{0}, \overset{i\text{th}}{\mathbf{k}}, \mathbf{0}, \dots, \mathbf{0}, \overset{j\text{th}}{-\mathbf{k}}, \mathbf{0}, \dots, \mathbf{0}), \forall \mathbf{k} \in \mathbb{R}^3\}.$$

In addition, if $\mathbf{K} \in \mathcal{S}_{ij}$, then only one term in the summation in (3.3) is nonzero, which is when the summation indices match those of the subspace \mathcal{S}_{ij} (unless $\mathbf{k} = \mathbf{0}$, in which case all terms in the summation are identical). For a system consisting of N particles, there are $N(N-1)/2$ such spaces \mathcal{S}_{ij} in total, each corresponding to an unordered pair of distinct particles.

Now that we have examined the structure of $\Phi_{\mathbf{K}}$, we can look at the structure of the forcing $(\mathbf{K}\Phi_{\mathbf{K}}) * \mathbf{W}_{\mathbf{K}}^T$. If we compare (3.2) with (3.3) and (3.5), it becomes clear that the nonzero values of the integrand in (3.2) are achieved for $\mathbf{K} - \mathbf{K}' \in \mathcal{S}_{ij}$. At the same time, $\mathbf{W}_{\mathbf{K}'}$ is the Fourier transform of the large scale flow velocity, and, therefore, is nonzero only for a set of small \mathbf{K}' , say, $\|\mathbf{K}'\| < b_W \ll \|\mathbf{K}\|$ (where b_W can be viewed as the ‘‘spectral bandwidth’’ of the strong large scale flow velocity \mathbf{W}). We conclude that the nonzero values of (3.2) lie in a *bundle*

$$(3.6) \quad \mathcal{B}_{ij} = \{\mathbf{K} - \mathbf{K}' \in \mathcal{S}_{ij}, \forall \|\mathbf{K}'\| < b_W\}.$$

It is clear that the bundle \mathcal{B}_{ij} is simply a relatively ‘‘thin’’ collection of translations of \mathcal{S}_{ij} around the origin to the distance of at most b_W . Also, any two distinct bundles \mathcal{B}_{ij} only intersect in a small region around zero (which corresponds to large scales), and are disjoint in the inertial range. Within each \mathcal{B}_{ij} , \mathbf{K} is roughly of the form (3.5), being somewhat ‘‘detuned’’ by at most b_W .

Lastly, let us assume that the Fourier transform $\phi_{\|\mathbf{k}\|}$ in (3.4) scales as some power of $\|\mathbf{k}\|$ in the inertial range. Then, it is obvious that, first, in $\Phi_{\mathbf{K}}$, given via (3.3), the same power scaling is shared across all subspaces \mathcal{S}_{ij} , defined by (3.5); and, second, that in the forcing (3.2), the same power scaling in the inertial range is shared across all bundles \mathcal{B}_{ij} , defined via (3.6). In what follows, this observation plays an important role.

3.1. The spatial structure of quantities induced by the potential forcing. Let us assume that a quantity, say A_K , is induced in the inertial range by the forcing in (3.2). Here, by “induced”, we do not necessarily mean that A_K equals the forcing in (3.2), but that, first, it is present on the same sets of K in the inertial range for which (3.2) is nonzero, and, second, its structure is largely governed by the scaling properties of the Fourier transform $\phi_{\|k\|}$ in the inertial range.

First, let us consider the situation where A_K is nonzero strictly in the subspaces \mathcal{S}_{ij} (3.5), but otherwise arbitrary. Here, we can assume that $K \neq \mathbf{0}$, since we are interested in the inertial range. Let a_K be some function of K , and let us write

$$(3.7) \quad A_K = \sum_{i=1}^{N-1} \sum_{j=i+1}^N a_K \delta(\mathbf{k}_i + \mathbf{k}_j) \prod_{\substack{m=1 \\ m \neq i,j}}^N \delta(\mathbf{k}_m).$$

Clearly, A_K is zero almost everywhere, with the exception for any K which belongs to one of the subspaces \mathcal{S}_{ij} . In the latter case, only one term in the sum above is nonzero (with indices i and j corresponding to the given subspace \mathcal{S}_{ij}), where A_K is given via a_K , scaled by the delta-functions. Since a_K is arbitrary, we can say that the form of A_K in (3.7) is the most general one which satisfies the requirement of being nonzero in \mathcal{S}_{ij} and zero otherwise. Next, let us introduce the following notation for convenience:

$$(3.8) \quad a_k^{ij} \stackrel{\text{def}}{=} \{a_K : K \in \mathcal{S}_{ij}\},$$

where k is the 3-dimensional wavevector parameter in the definition of \mathcal{S}_{ij} in (3.5). With this notation, we can write (3.7) as

$$(3.9) \quad A_K = \sum_{i=1}^{N-1} \sum_{j=i+1}^N a_{k_i}^{ij} \delta(\mathbf{k}_i + \mathbf{k}_j) \prod_{\substack{m=1 \\ m \neq i,j}}^N \delta(\mathbf{k}_m).$$

Reverting the procedure in Appendix A, we find that the inverse Fourier transform $A(\mathbf{X})$ of A_K , whose form is specified in (3.7)–(3.9), is given via

$$(3.10) \quad A(\mathbf{X}) = \sum_{i=1}^{N-1} \sum_{j=i+1}^N a^{ij}(\mathbf{x}_i - \mathbf{x}_j),$$

where $a^{ij}(\mathbf{x})$ is the 3-dimensional inverse Fourier transform of a_k^{ij} . We can see that, in the most general form, $A(\mathbf{X})$ depends on the differences of coordinates of all unordered pairs of particles. One of the consequences of such a dependence is that $A(\mathbf{X})$ is invariant under a coordinate system shift in the physical 3D-space which is occupied by particles. Indeed, if we add the same offset to the location \mathbf{x}_i of each particle, then the differences $\mathbf{x}_j - \mathbf{x}_i$ will remain the same, and thus $A(\mathbf{X})$ in (3.10) will not change.

Similarly, we can also presume that A_K is nonzero in the bundles \mathcal{B}_{ij} of (3.6). In this case, similarly to (3.2), A_K can be expressed in the form of a convolution of (3.7)–(3.9) with some large scale variable, whose spectral bandwidth is the same as that of W_K in (3.2). In the physical space, this will become (3.10), multiplied by the inverse Fourier transform of that large scale variable. If the large scale structures are filtered out, the remainder will have the form in (3.10).

Next, let us examine what happens to (3.10) in the framework of conventional fluid dynamics. Recall that the Boltzmann equation [1, 3, 9] is obtained from the Liouville equation in (2.6) via the BBGKY formalism [2, 4, 20], by integrating the probability density F over the coordinates and velocities of all particles but one, obtaining the single-particle marginal distribution f_1 :

$$(3.11) \quad f_1(\mathbf{x}_1, \mathbf{v}_1) = \int_{\mathbb{R}^{6(N-1)}} F(\mathbf{X}, \mathbf{V}) d\mathbf{x}_2 \dots d\mathbf{x}_N d\mathbf{v}_2 \dots d\mathbf{v}_N.$$

It is then presumed that all particles are distributed identically, and thus the coordinates \mathbf{x}_1 and \mathbf{v}_1 of the first particle are taken to be the coordinates of “any” particle, so that all subscripts in (3.11) are dropped. The Boltzmann equation is the corresponding transport equation for $f(\mathbf{x}, \mathbf{v})$. The Euler and Navier–Stokes equations are obtained by further integrating f against various powers of \mathbf{v} , just as we have done above in (2.12) for the complete system of particles.

If we apply the BBGKY procedure to (3.10) and integrate over all coordinates but \mathbf{x}_i for some i , $1 \leq i \leq N$, it is obvious that the resulting quantity will be a constant. Note, however, that this happens solely due to the fact that the classical BBGKY formalism is applied to a single particle. If the BBGKY formalism is applied, say, to the joint distribution of two particles (that is, the averaging is performed over all particles but two), then one 3-dimensional subspace \mathcal{S}_{ij} in (3.5) will be preserved, which corresponds to this pair of particles. Similarly, if the BBGKY formalism is applied to the joint distribution of K particles, then $K(K-1)/2$ such subspaces will be preserved, each corresponding to an unordered pair of these K particles.

At this point, it is clear that the subspaces \mathcal{S}_{ij} in (3.5), and the corresponding bundles \mathcal{B}_{ij} in (3.6), are destroyed in the single-particle BBGKY formalism of the conventional fluid dynamics, together with all quantities of the form (3.10), induced by the strong large scale flow in the inertial range via the potential interaction. For comparison, let us examine whether these quantities can be captured in the process of measurement of an actual gas flow. Here, we assume that there is a grid of M measurement points, with coordinate offsets between them given via $(\mathbf{y}_1, \dots, \mathbf{y}_{M-1})$. We also assume that the number of particles N is much greater than the number of measurement points M (for example, $M \sim 10^3$, while $N \sim 10^{23}$). Each measurement point contains a “probe” (that is, a measurement device), which interacts with all particles which happen to pass through that location, and measures their physical property of interest.

In the course of the measurement, each probe registers the particles which pass through that probe’s location. Those particles which do not pass through any of the probes, are not measured at all. Thus, the measurement registers M distinct sets of particles, the distances between which given via \mathbf{y}_m . Since the probes do not discern between individual particles, the quantity which will be recorded constitutes the ensemble average over the particles, whose coordinates, as well as the differences between them are known at the time of the measurement:

$$(3.12) \quad \langle A \rangle(\mathbf{y}_m) = \text{ensemble average over all pairs } A(\mathbf{x}_j - \mathbf{x}_i = \mathbf{y}_m).$$

Thus, the offsets of measurement grid points \mathbf{y}_m encode the differences between particle’s locations, which is what $A(\mathbf{X})$ in (3.10) depends on. Also, each pair of particles (say

i th and j th), registered at a location m , samples a single point from their corresponding bundle \mathcal{B}_{ij} from (3.6). However, since the number of registered pairs (and, therefore, their respective bundles \mathcal{B}_{ij}) is large at any location m , the quantity which is measured constitutes the ensemble average over these bundles, which are effectively “collapsed” into the single 3-dimensional space sampled via \mathbf{y}_m . While a lot of information is lost during this collapse (for example, the phases of individual particle locations), the bulk information, such as the power scaling of A_K shared between all bundles \mathcal{B}_{ij} , should remain largely preserved. It is thus obvious that the subsequent discrete Fourier transformation (DFT) of such a collapsed measurement will reveal the same power scaling as shared across all bundles \mathcal{B}_{ij} in (3.6). Thus, so far we can summarize that:

- a. Via the interaction potential, the velocity of a strong large scale flow creates forcing in the inertial range, which is located in the bundles \mathcal{B}_{ij} given via (3.6), which themselves consist of subspaces \mathcal{S}_{ij} , given via (3.5);
- b. In the conventional fluid dynamics, these bundles are destroyed by the BBGKY formalism [2, 4, 20], which leads from the Liouville equation (2.6) to the Boltzmann equation [1, 3, 9];
- c. The measurements of the flow, however, can register quantities which live in these bundles. While a measurement collapses these bundles into the measurement 3-dimensional space, certain bulk properties can still manifest in the measured data.

In what follows, we crudely estimate the scaling of the energy spectra in the bundles \mathcal{B}_{ij} , based on a realistic choice of the interaction potential $\phi(r)$, and compare the estimates against some known measurements.

4. WEIGHTED TIME AVERAGING OF THE LIOUVILLE EQUATION

Above, we found that a strong large scale flow induces a forcing at the inertial scales via an interaction potential. This forcing, however, lives in special bundles \mathcal{B}_{ij} of the form (3.6), which are shared by pairs of particles. Due to such a structure, these bundles are not present in the equations of conventional fluid dynamics, such as the Boltzmann, Euler and Navier–Stokes equations, as they are destroyed in the process of the BBGKY formalism [2, 4, 20]. However, if an observation of this flow is performed via a grid of measurement probes, then some bulk properties of the flow shared across these bundles (such as, for example, the power scaling with the Fourier wavenumber), can be captured by the probes. This suggests that if a strong large scale flow indeed causes the turbulent motions at the inertial scales by means of the discovered forcing, then it would be interesting to estimate, for example, the power scaling of the kinetic energy in these bundles, and compare it with the observations.

Recall that turbulent kinetic energy spectra are observed for windowed time averages of observed flows [30]. Thus, in order to find out whether such spectra can manifest in the N -particle model (2.3), we need to transform the Liouville equation in (2.6) in such a way so that the resulting relations describe either a windowed time average, or at least something similar to it. Observe that (2.6) is a linear PDE, and thus the straightforward application of a windowed time average on both sides transforms any instance of F into the corresponding time average – except for the time-derivative term, which becomes the

difference between the initial and terminal states of F . This is somewhat inconvenient, since the terminal condition cannot simply be ignored or set to zero (note that F is a probability density, and thus it is nonnegative and must integrate to 1).

Here, instead, to express the weighted time average of F , we will use the quantity

$$(4.1) \quad \bar{F}(T, \mathbf{X}, \mathbf{V}) = \frac{1}{T} \int_0^\infty F(t, \mathbf{X}, \mathbf{V}) e^{-t/T} dt,$$

where $T > 0$ is a parameter. Observe that, for any T , $\bar{F}(T, \mathbf{X}, \mathbf{V})$ is also a probability density; indeed, first, $\bar{F}(T, \mathbf{X}, \mathbf{V}) \geq 0$ (obviously), and, second,

$$(4.2) \quad \int \bar{F}(T, \mathbf{X}, \mathbf{V}) d\mathbf{X} d\mathbf{V} = \frac{1}{T} \int_0^\infty F(t, \mathbf{X}, \mathbf{V}) e^{-t/T} dt d\mathbf{X} d\mathbf{V} = \frac{1}{T} \int_0^\infty e^{-t/T} dt = 1.$$

While $\bar{F}(T, \mathbf{X}, \mathbf{V})$ is not exactly the windowed time average of F , it is qualitatively similar to the latter – even though there is no rigid cut-off at T in the upper limit of the integral, a “soft cut-off” is present in the form of the exponential weight with the characteristic scale T . Additionally, for large T , $\bar{F}(T, \mathbf{X}, \mathbf{V})$ indeed approaches the time average of F :

$$(4.3) \quad \lim_{T \rightarrow \infty} \bar{F}(T, \mathbf{X}, \mathbf{V}) = \lim_{T \rightarrow \infty} \frac{1}{T} \int_0^T F(t, \mathbf{X}, \mathbf{V}) dt.$$

The proof of (4.3) can be found in [16]; we also provide it in Appendix B below.

Next, recall that the Laplace transform $\mathcal{L}\{F\}(s, \mathbf{X}, \mathbf{V})$ of the probability density F is given via

$$(4.4) \quad \mathcal{L}\{F\}(s, \mathbf{X}, \mathbf{V}) = \int_0^\infty F(t, \mathbf{X}, \mathbf{V}) e^{-st} dt.$$

Now, observe that, if we set $T = s^{-1}$, then $\bar{F}(T, \mathbf{X}, \mathbf{V})$ is the same as $s\mathcal{L}\{F\}(s, \mathbf{X}, \mathbf{V})$:

$$(4.5) \quad \bar{F}(s^{-1}, \mathbf{X}, \mathbf{V}) = s \int_0^\infty F(t, \mathbf{X}, \mathbf{V}) e^{-st} dt = s\mathcal{L}\{F\}(s, \mathbf{X}, \mathbf{V}).$$

With the latter observation, it is easy to transform the Liouville equation in (2.6) into the corresponding equation for \bar{F} . First, we apply the Laplace transformation on both sides of the Liouville equation in (2.6):

$$(4.6) \quad s\mathcal{L}\{F\} - F_0 + \mathbf{V} \cdot \frac{\partial}{\partial \mathbf{X}} \mathcal{L}\{F\} = \frac{\partial \Phi}{\partial \mathbf{X}} \cdot \frac{\partial}{\partial \mathbf{V}} \mathcal{L}\{F\},$$

where $F_0 = F(0, \mathbf{X}, \mathbf{V})$ is the initial condition for F . Then, multiplying both sides by s and denoting $T = s^{-1}$, we arrive at

$$(4.7) \quad \frac{1}{T} (\bar{F} - F_0) + \mathbf{V} \cdot \frac{\partial \bar{F}}{\partial \mathbf{X}} = \frac{\partial \Phi}{\partial \mathbf{X}} \cdot \frac{\partial \bar{F}}{\partial \mathbf{V}}.$$

Since \bar{F} is a probability density, the same techniques can be applied for (4.7), as above for (2.6). Denoting the corresponding Laplace-averaged velocity moments for \bar{F} via $\bar{\rho}$, $\bar{\mathbf{U}}$, $\bar{\mathbf{E}}$, $\bar{\mathbf{Q}}$ and $\bar{\mathbf{R}}$, we obtain the following Laplace-averaged moment equations:

$$(4.8a) \quad \frac{1}{T} (\bar{\rho} - \rho_0) + \frac{\partial}{\partial \mathbf{X}} \cdot (\bar{\rho} \bar{\mathbf{U}}) = 0, \quad \frac{1}{T} (\bar{\rho} \bar{\mathbf{U}} - \rho_0 \mathbf{U}_0) + \frac{\partial}{\partial \mathbf{X}} \cdot (\bar{\rho} \bar{\mathbf{E}}) = -\bar{\rho} \frac{\partial \Phi}{\partial \mathbf{X}},$$

$$(4.8b) \quad \frac{1}{T}(\bar{\rho}\bar{\mathbf{E}} - \rho_0\mathbf{E}_0) + \frac{\partial}{\partial\mathbf{X}} \cdot (\bar{\rho}(\bar{\mathbf{Q}} + \bar{\mathbf{R}})) = -\bar{\rho} \left(\frac{\partial\Phi}{\partial\mathbf{X}}\bar{\mathbf{U}}^T + \bar{\mathbf{U}} \frac{\partial\Phi}{\partial\mathbf{X}} \right).$$

Further applying the Fourier transformation in \mathbf{X} to (4.8) in the same manner as was done in (2.14), we arrive at

$$(4.9a) \quad \frac{1}{\hat{i}T}(\bar{\rho}_K - \rho_{0,K}) + \mathbf{K} \cdot (\bar{\rho}_K * \bar{\mathbf{U}}_K) = 0,$$

$$(4.9b) \quad \frac{1}{\hat{i}T}(\bar{\rho}_K * \bar{\mathbf{U}}_K - \rho_{0,K} * \mathbf{U}_{0,K}) + \mathbf{K} \cdot (\bar{\rho}_K * \bar{\mathbf{E}}_K) = -\bar{\rho}_K * (\mathbf{K}\Phi_K),$$

$$(4.9c) \quad \frac{1}{\hat{i}T}(\bar{\rho}_K * \bar{\mathbf{E}}_K - \rho_{0,K} * \mathbf{E}_{0,K}) + \mathbf{K} \cdot (\bar{\rho}_K * (\bar{\mathbf{Q}}_K + \bar{\mathbf{R}}_K)) = \\ = -\bar{\rho}_K * \left[(\mathbf{K}\Phi_K) * \bar{\mathbf{U}}_K^T + \bar{\mathbf{U}}_K * (\mathbf{K}\Phi_K)^T \right].$$

For the same assumptions as in (3.1), in the inertial range we obtain

$$(4.10a) \quad \frac{1}{\hat{i}T}\bar{\rho}_K + \mathbf{K} \cdot (\bar{\rho}_K * \bar{\mathbf{U}}_K) = 0, \quad \frac{1}{\hat{i}T}\bar{\rho}_K * \bar{\mathbf{U}}_K + \mathbf{K} \cdot (\bar{\rho}_K * \bar{\mathbf{E}}_K) = 0,$$

$$(4.10b) \quad \frac{1}{\hat{i}T}\bar{\rho}_K * \bar{\mathbf{E}}_K + \mathbf{K} \cdot (\bar{\rho}_K * (\bar{\mathbf{Q}}_K + \bar{\mathbf{R}}_K)) = -\bar{\rho}_K * \left[(\mathbf{K}\Phi_K) * \bar{\mathbf{W}}_K^T + \bar{\mathbf{W}}_K * (\mathbf{K}\Phi_K)^T \right],$$

where $\bar{\mathbf{W}}_K$ is the Laplace average of the strong large scale velocity \mathbf{W}_K in (3.1), and we recall that the initial values $\rho_{0,K}$, $\mathbf{U}_{0,K}$ and $\mathbf{E}_{0,K}$ in the inertial range are presumed to be zero.

5. SIMPLIFIED RELATIONS AND SCALING ESTIMATES FOR THE INERTIAL RANGE

In what follows, our goal is to estimate bulk power scaling relations in the bundles \mathcal{B}_{ij} from (3.6) between the Fourier transform $\phi_{\|k\|}$ of the interaction potential and the Fourier transform $\bar{\mathbf{E}}_K$ of the Laplace-averaged kinetic energy, and compare the estimates with the observations. Here, we must keep in mind that what is observed is not necessarily the exact solution, but rather the most “visible” component of the solution. For example, when a power scaling of the kinetic energy is observed, it does not necessarily mean that the solution has a precise power scaling form – but rather that its other components may decay faster than that, and thus be less “visible”. Additionally, it is known that, in a large variety of configurations of the large scale flow, the turbulent motions do not manifest themselves at all (this is known as the “laminar” flow). Therefore, for the purpose of this work, further we will tacitly assume that the large scale flow configuration is such that the turbulent motions arise, and will focus specifically on the estimates which yield the bulk power scaling of the kinetic energy spectra, while keeping in mind that other, more rapidly decaying, components of the solution could also be “invisibly” present.

Since we do not need to look for exact solutions of (4.10), we can instead identify dominant terms in (4.10) and crudely estimate the order-of-magnitude relations between them. For that, we make the following simplifying assumptions in (4.10):

- a. On the chosen averaging time scale T , the flow is effectively incompressible, that is, $\bar{\rho}_K$ is confined to a very narrow wavenumber range $\|K\| \ll 1$, and thus can be factored out of the convolution integrals – in fact, this is what is observed in practice for many turbulent flows;
- b. On the chosen averaging time scale T , the skewness moment $\bar{\mathbf{Q}}_K$ in the inertial range can be neglected in comparison with the combination of the velocity and energy moments $\bar{\mathbf{R}}_K$ – as we mentioned above, in practical scenarios, the skewness and higher-order non-Gaussian moments typically manifest themselves at viscous scales, while in the inertial range the non-Gaussian moments are small;
- c. In the energy equation, the Fourier transform $\bar{\mathbf{E}}_K$ decays faster with K than the remaining part of the advection term $K \cdot \bar{\mathbf{R}}_K$, and thus can be neglected in the inertial range. This assumption will be shown to hold for all estimates below.

The resulting simplified relations for the velocity and energy are given via

$$(5.1) \quad \bar{\mathbf{U}}_K \approx -\hat{i}TK \cdot \bar{\mathbf{E}}_K, \quad K \cdot \bar{\mathbf{R}}_K \approx -(K\Phi_K) * \bar{\mathbf{W}}_K^T - \bar{\mathbf{W}}_K * (K\Phi_K)^T.$$

Below, we will assume that the scaling of the Fourier transforms $\bar{\mathbf{U}}_K$ and $\bar{\mathbf{E}}_K$ in the bundles \mathcal{B}_{ij} from (3.6) with k (where k is the wavevector parameter in (3.5)) is governed by these approximate relations in (5.1).

Next, since the nonzero values of the Laplace-averaged strong large scale flow velocity $\bar{\mathbf{W}}_K$ are confined to a small ball $\|K\| < b_W$, we observe that, in any bundle \mathcal{B}_{ij} from (3.6) the scaling of $\bar{\mathbf{R}}_K$ should be the same as the scaling of $\phi_{\|k\|}$, with K within \mathcal{B}_{ij} in the inertial range being roughly of the form in (3.5):

$$(5.2) \quad K \cdot \bar{\mathbf{R}}_K \sim K\phi_{\|k\|}, \quad \text{or} \quad \bar{\mathbf{R}}_K \sim \phi_{\|k\|}.$$

Recall that $\bar{\mathbf{R}}_K$ itself consists of convolutions of $\bar{\mathbf{U}}_K$ with itself and $\bar{\mathbf{E}}_K$. Thus, even though the scaling of $\bar{\mathbf{R}}_K$ in a bundle \mathcal{B}_{ij} is fully determined via (5.2), the convolutions $\bar{\mathbf{U}}_K \circledast \bar{\mathbf{E}}_K$ and $\bar{\mathbf{U}}_K \circledast \bar{\mathbf{U}}_K \circledast \bar{\mathbf{U}}_K$ can, in principle, combine the contributions from different bundles. Besides, even though $\bar{\mathbf{R}}_K$ is zero when $K \notin \mathcal{B}_{ij}$, it does not mean that $\bar{\mathbf{U}}_K$ and $\bar{\mathbf{E}}_K$ are necessarily zero for the same K . Ultimately, not every flow is necessarily turbulent, even if it does have a strong large scale velocity component.

Therefore, in what follows, we will consider the solutions $\bar{\mathbf{U}}_K$ and $\bar{\mathbf{E}}_K$ of (4.10) and (5.1), which have the same bulk structure as that of $\bar{\mathbf{R}}_K$ (that is, they are nonzero in the bundles \mathcal{B}_{ij} and zero otherwise). Additionally, we will assume that the values of $\bar{\mathbf{R}}_K$ in a bundle \mathcal{B}_{ij} are largely determined by the values of $\bar{\mathbf{U}}_K$ and $\bar{\mathbf{E}}_K$ in that same bundle, that is, the contribution of convolutions across distinct bundles is either negligible, or at least does not affect the scaling significantly. To make the scaling estimates, we will also assume that the double velocity convolution in the formula for $\bar{\mathbf{R}}_K$ in (2.15) scales in the same manner as $\bar{\mathbf{R}}_K$ itself in (5.2),

$$(5.3) \quad \bar{\mathbf{U}}_K \circledast \bar{\mathbf{U}}_K \circledast \bar{\mathbf{U}}_K \sim \bar{\mathbf{R}}_K \sim \phi_{\|k\|},$$

in any bundle \mathcal{B}_{ij} . Just as the assumption about the energy decay above, this assumption will be shown to hold for all estimates below.

Given the sparse structure of Φ_K in (3.3), observe that the convolution in (3.2) qualitatively replicates the pattern of the strong large scale flow velocity $\bar{\mathbf{W}}_K$ along the bundles

\mathcal{B}_{ij} in (3.6). While this pattern is not copied verbatim (as the term $K\Phi_K$ adjusts the scaling with K), it is clear that some qualitative degree of “self-similarity” must be present in (3.2) across the inertial range. If the relation in (5.3) holds, then one can expect such self-similar patterns to also manifest in the inverse Fourier transform of the Laplace-averaged velocity \bar{U}_K . This is what seems to be usually observed in turbulent flows.

In order to make the scaling estimates of the Fourier transforms of the velocity and energy, below we separate the inertial range into the following two subranges:

- a. **Large scale inertial subrange** – this is the subrange of the Fourier wavenumbers adjacent to the large scale flow;
- b. **Small scale inertial subrange** – this is the subrange of the Fourier wavenumbers adjacent to the viscous range.

This separation must be put in place due to the presence of the velocity cut-off in the viscous spatial range – as we show below, the scaling estimates must be computed differently, depending on how far away the wavenumber is from the viscous velocity cut-off.

5.1. Scaling estimate for the large scale inertial subrange. Above, we assumed that a physically relevant solution of (2.14) has a cut-off for the Fourier transform of the velocity at the boundary of the viscous range. However, for a Fourier wavenumber K which is in the inertial range, but in the proximity of the large scale flow, the effect of the viscous cut-off can be very small, since it happens on a much smaller scale. In such a case, one can assume that the viscous cut-off is not present, and, therefore, to estimate the scaling of the velocity and energy in the inertial range near the large scale flow, we can use the standard regularity estimates from the Fourier analysis.

Let us write the expression for the double convolution explicitly via the corresponding integral:

$$(5.4) \quad \bar{U}_K \circledast \bar{U}_K \circledast \bar{U}_K = \int_{\mathbb{R}^{3N}} \int_{\mathbb{R}^{3N}} \bar{U}_{K-K'} \otimes \bar{U}_{K'-K''} \otimes \bar{U}_{K''} dK'' dK'.$$

Clearly, if $\|K\|$ is much smaller than the threshold for the viscous cut-off, then, even in the absence of the cut-off, due to power decay, the contribution from the small scale wavenumbers is much smaller than from those which surround K . Subsequently, the result of the double convolution in (5.4) without the viscous cut-off should not be much different from that with the cut-off present.

In such a situation, we can ignore the velocity cut-off at viscous scales, and proceed as if the scaling of \bar{U}_K and \bar{R}_K above in (5.2) and (5.3) extends onto all Fourier wavenumbers. This scaling, in turn, determines the regularity class for \bar{R} itself, which is the inverse Fourier transform of \bar{R}_K . At the same time, the convolution in the Fourier space becomes the product in the physical space:

$$(5.5) \quad \bar{R} \sim \bar{U} \otimes \bar{U} \otimes \bar{U}.$$

Since \bar{R} is, effectively, a cubic power of \bar{U} , it means that \bar{U} belongs to the same regularity class as \bar{R} . This, in turn, means that, for $\|K\|$ in the inertial range near the large scales, \bar{U}_K should scale in the same manner as \bar{R}_K along any bundle \mathcal{B}_{ij} :

$$(5.6) \quad \bar{U}_K \sim \bar{R}_K \sim \phi_{\|k\|}.$$

However, due to (5.1), the latter means that the scaling for the energy $\bar{\mathbf{E}}_K$ is given via

$$(5.7) \quad \bar{\mathbf{E}}_K \sim \frac{\phi_{\|k\|}}{\|k\|},$$

along any bundle \mathcal{B}_{ij} from (3.6). It remains to be verified that the obtained scaling does not violate the assumptions in (5.1) and (5.3). Indeed, observe that, since $\bar{\mathbf{E}}$ is in the “better” regularity class than $\bar{\mathbf{U}}$, the product $\bar{\mathbf{U}} \otimes \bar{\mathbf{E}}$ (which is what becomes of convolutions $\bar{\mathbf{U}}_K \circledast \bar{\mathbf{E}}_K$ in the coordinate space) falls into the same regularity class as $\bar{\mathbf{U}}$ itself. Thus, we conclude that all terms in $\bar{\mathbf{R}}_K$ scale in the same fashion within the inertial range near the large scale flow, which ascertains the validity of (5.3). Also, $\bar{\mathbf{E}}_K$ indeed decays faster with K than $K \cdot \bar{\mathbf{R}}_K$, so that (5.1) remains valid.

5.2. Scaling estimate for the small scale inertial subrange. If the wavenumber K in (5.1) is in the vicinity of the viscous velocity cut-off, the regularity estimates above cannot be used. The reason for this is that the velocity convolutions in $\bar{\mathbf{R}}_K$ have a limited effective domain of integration, which completely changes the scaling behavior of the convolvent. To illustrate this, let us shift the dummy variables of integration in (5.4) as follows:

$$(5.8) \quad K' \rightarrow K' + 2K/3, \quad K'' \rightarrow K'' + K/3.$$

This change of the variables of integration leads to

$$(5.9) \quad \bar{\mathbf{U}}_K \circledast \bar{\mathbf{U}}_K \circledast \bar{\mathbf{U}}_K = \int_{\mathbb{R}^{3N}} \int_{\mathbb{R}^{3N}} \bar{\mathbf{U}}_{K/3-K'} \otimes \bar{\mathbf{U}}_{K/3+K'-K''} \otimes \bar{\mathbf{U}}_{K/3+K''} dK'' dK'.$$

Now it is easy to see that if $K/3$ above is chosen near the viscous velocity cut-off, then the values of K' and K'' , for which the integrand is nonzero, are clustered in a small region around zero. In order to see how the power scaling of the convolution is affected, let us assume that $\bar{\mathbf{U}}_K$ has the form

$$(5.10) \quad \bar{\mathbf{U}}_K = \|K\|^{-\gamma} \mathbf{Y}_K,$$

where $\gamma > 0$ is a power scaling constant, while \mathbf{Y}_K scales as $O(1)$ in the inertial range, and rapidly decays to zero beyond the viscous cut-off. Upon substitution of (5.10) into (5.9), we arrive at

$$(5.11) \quad \bar{\mathbf{U}}_K \circledast \bar{\mathbf{U}}_K \circledast \bar{\mathbf{U}}_K = \int_{\mathbb{R}^{3N}} \int_{\mathbb{R}^{3N}} (\|K/3 - K'\| \|K/3 + K' - K''\| \|K/3 + K''\|)^{-\gamma} \mathbf{Y}_{K/3-K'} \otimes \mathbf{Y}_{K/3+K'-K''} \otimes \mathbf{Y}_{K/3+K''} dK'' dK'.$$

At this point, it is already clear that, if K' and K'' above are confined to a small region around zero, the product of norms above can be expected to scale as $\|K\|^{-3\gamma}$. To

elaborate more on this estimate, we first write, for the product of norms alone,

$$(5.12) \quad \begin{aligned} & \|K/3 - K'\| \|K/3 + K' - K''\| \|K/3 + K''\| = \\ &= \frac{\|K\|^3}{27} \left[\left(1 - \frac{6K^T K'}{\|K\|^2} + \frac{9\|K'\|^2}{\|K\|^2}\right) \left(1 + \frac{6K^T(K' - K'')}{\|K\|^2} + \frac{9\|K' - K''\|^2}{\|K\|^2}\right) \right. \\ & \quad \left. \left(1 + \frac{6K^T K''}{\|K\|^2} + \frac{9\|K''\|^2}{\|K\|^2}\right) \right]^{1/2} = \frac{\|K\|^3}{27} \sqrt{G\left(\frac{2K}{\|K\|}, \frac{3K'}{\|K\|}, \frac{3K''}{\|K\|}\right)}, \end{aligned}$$

where $G(a, b, c)$ is given via

$$(5.13) \quad \begin{aligned} G(a, b, c) &= (1 - a^T b + \|b\|^2)(1 + a^T(b - c) + \|b - c\|^2)(1 + a^T c + \|c\|^2) = \\ &= 1 + \|b\|^2 + \|c\|^2 + \|b - c\|^2 + (b - a)^T b (a + c)^T c + (b - a)^T b (a + b - c)^T (b - c) + \\ & \quad + (a + b - c)^T (b - c) (a + c)^T c + (b - a)^T b (a + b - c)^T (b - c) (a + c)^T c, \end{aligned}$$

and notably lacks the linear terms in b and c , since they cancel out due to the alternating signs. The form of G above results in the order-of-magnitude behavior

$$(5.14) \quad G\left(\frac{2K}{\|K\|}, \frac{3K'}{\|K\|}, \frac{3K''}{\|K\|}\right) = 1 + O\left(\frac{\|K'\|^2}{\|K\|^2}\right) + O\left(\frac{\|K''\|^2}{\|K\|^2}\right) + O\left(\frac{\|K\|\|K''\|}{\|K\|^2}\right),$$

that is, for $\|K'\| \sim \|K''\| \ll \|K\|$, G behaves similarly to a constant, with at least a quadratic correction term. The convolution thus becomes

$$(5.15) \quad \begin{aligned} \bar{U}_K \circledast \bar{U}_K \circledast \bar{U}_K &= \frac{27^\gamma}{\|K\|^{3\gamma}} \int_{\mathbb{R}^{3N}} \int_{\mathbb{R}^{3N}} G\left(\frac{2K}{\|K\|}, \frac{3K'}{\|K\|}, \frac{3K''}{\|K\|}\right)^{-\gamma/2} \\ & \quad Y_{K/3-K'} \otimes Y_{K/3+K'-K''} \otimes Y_{K/3+K''} dK'' dK'. \end{aligned}$$

Even though G behaves like a constant, and Y_K is $O(1)$, the full integral above does not necessarily scale like a constant in K . This happens because the size of the effective domain of integration depends on K too – indeed, the farther away is $\|K\|$ from the viscous cut-off, the larger is the effective domain of integration (whose size scales as a power of the difference between $\|K\|$ and the viscous cut-off). If the integral scales proportionally to the effective domain of the integration, on a log-log plot, such a dependence will look like a rapidly, superlinearly decreasing function of $\|K\|$, and thus the power scaling in $\|K\|$ cannot be achieved in such a case.

Therefore, in order to attain the power scaling in $\|K\|$, the magnitude of the integral in (5.15) should not scale with the size of the domain of integration. This can be achieved if Y_K consists of self-similar patterns with alternating signs, so that appropriate cancellations can occur during the integration. Such an ansatz seems to be supported by observations, where turbulent structures usually consist of chaotically oriented self-similar eddies spanning multiple scales. Also, since the structure of Y_K is determined by the structure of the strong large scale flow \bar{W}_K , the latter should likely have a suitable pattern to induce a turbulent flow – clearly, not all large scale flows necessarily produce turbulent effects. Therefore, a naturally emerging (and likely difficult) problem here is

to determine a variety of patterns for \bar{W}_K which can produce appropriate forcings via (3.2), so that the resulting velocity fields have the suitable self-canceling structure.

At this point, what remains to be determined is the corresponding energy scaling. Clearly, if K belongs to a bundle \mathcal{B}_{ij} in (3.6), then so does $K/3$. Thus, combining (5.3), (5.10) and (5.15), we arrive at

$$(5.16) \quad \|K\|^{-3\gamma} \sim \phi_{\|k\|}, \quad \text{and, therefore,} \quad \bar{U}_K \sim \|K\|^{-\gamma} \sim \sqrt[3]{\phi_{\|k\|}},$$

where k is the wavevector which parameterizes the bundle \mathcal{B}_{ij} in (3.6) via (3.5). Due to (5.1), the latter means that, in the small scale inertial range near the viscous velocity cut-off, the energy scales as

$$(5.17) \quad \bar{E}_K \sim \frac{\sqrt[3]{\phi_{\|k\|}}}{\|k\|}.$$

Lastly, we have to verify that, for the obtained scaling, the assumptions above in (5.1) and (5.3) indeed hold. Here, since $K/3$ is chosen to be near the viscous cut-off for \bar{U}_K , and \bar{E}_K is given via (5.1) (and is a ‘‘multiple’’ of the velocity), then the convolution of \bar{U}_K with \bar{E}_K at most reaches the wavenumber $2K/3$, and never K itself. Thus, around K , \bar{R}_K consists only of the double velocity convolution, which ascertains (5.3). Similarly, the energy \bar{E}_K alone can never extend beyond $K/3$, which means that the only quantity affected by the forcing near K in (5.1) is \bar{R}_K .

6. THE CHOICE OF THE INTERACTION POTENTIAL AND THE SCALING ESTIMATES

Above in (5.6), (5.7), (5.16) and (5.17), we obtained the estimates for the velocity and energy scaling in the inertial range, which depend on the scaling of the Fourier transform $\phi_{\|k\|}$ of the interaction potential $\phi(r)$. Here, we need to choose the form of $\phi(r)$, which would provide a realistic Fourier transform in (3.4). The main problem here is that, in reality, the interactions between molecules are largely governed by quantum-mechanical effects (in particular, the Pauli exclusion principle). An ‘‘interaction potential’’ is merely the averaged, statistical manifestation of the latter in the classical limit, and, therefore, no potential fully describes the interactions between real-world molecules.

Typically, the choice of a potential is defined by the context of a relevant problem. For example, the widely known Buckingham [7] and Lennard-Jones [25] potentials are constructed using semi-empirical reasoning for the dynamics of low-energy, densely packed atoms primarily in liquids, and do not generally provide an accurate description outside of this context. In particular, the main focus of both the Lennard-Jones and Buckingham potentials is on the accuracy of the attracting term, which is known, from experiments and observations, to scale as $\sim r^{-6}$ with the distance. On the other hand, the repulsion terms of the aforementioned potentials, which are important for the high-energy collisions in a ‘‘normal’’ gas, are chosen largely out of convenience. As a result, not only the Fourier integrals of both the Lennard-Jones and Buckingham potentials are unbounded due to near-zero singularities, but even if they were somehow made bounded (say, via a suitable regularization limit), they would have been effectively unrelated.

In the present context, our goal is to choose the potential model which offers a realistic scaling of the Fourier transform. This means that the qualitative, bulk behavior of the

potential must be physically reasonable, instead of being quantitatively tailored to a particular narrow range of scales and energies. At the same time, the model must be sufficiently simple, to allow explicit treatment without the need to resort to numerical simulations. Arguably, the simplest model of this kind is the Thomas–Fermi model [13, 37], which is based upon a (rather crude) quantum-mechanical formulation of the atomic structure via Schrödinger’s equation. According to the Thomas–Fermi model, the potential $\phi(r)$ has the form

$$(6.1) \quad \phi(r) = \frac{\phi_0}{r} \eta\left(\frac{r}{\sigma}\right),$$

where ϕ_0 is a dimensional constant, $\eta(r)$ is a screening function, and σ is the characteristic screening distance. The screening function $\eta(r)$ satisfies the Thomas–Fermi nonlinear differential equation:

$$(6.2) \quad \frac{d^2\eta}{dr^2} = \sqrt{\frac{\eta^3}{r}}, \quad \eta(0) = 1, \quad \eta(\infty) = 0.$$

Note that the solution to the Thomas–Fermi equation is unavailable in the explicit form. However, in order to estimate the scaling of the Fourier transform $\phi_{\|\mathbf{k}\|}$, we only need to know certain properties of the solution. It is known [21, 36] that, for $0 \leq r < \infty$, $\eta(r)$ is a bounded strictly positive monotonically decreasing function, which behaves asymptotically as $\sim 144r^{-3}$ for $r \rightarrow \infty$. It also possesses continuous bounded strictly negative monotonically increasing derivative, whose initial value $\eta'(0) \approx -1.588$. Thus, the Thomas–Fermi potential itself behaves as $\sim r^{-1}$ for $r \ll 1$, and $\sim r^{-4}$ for $r \gg 1$.

6.1. The scaling for the Thomas–Fermi potential. Substituting (6.1) into (3.4), and rescaling $r \rightarrow \sigma r$, we obtain

$$(6.3) \quad \phi_{\|\mathbf{k}\|} = \frac{2\phi_0\sigma}{\|\mathbf{k}\|} \int_0^\infty \eta(r) \sin(2\pi\sigma\|\mathbf{k}\|r) dr.$$

Above, the integral alone is the Fourier sine transform of a continuously differentiable function on the right half-axis with a discontinuous odd extension. Therefore, it scales as $(\sigma\|\mathbf{k}\|)^{-1}$ as $\|\mathbf{k}\| \rightarrow \infty$, which, in turn, means that the Fourier transform $\phi_{\|\mathbf{k}\|}$ in (6.3) should scale as $\|\mathbf{k}\|^{-2}$ as $\|\mathbf{k}\| \rightarrow \infty$.

For a more accurate estimate, let us first note that, for $\sigma\|\mathbf{k}\| \ll 1$ (which corresponds to large scales) we can assume that $\eta(r)$ decays to zero much faster than the scale of variation of the sine function. In such a case, we can truncate the sine function to its own leading order Taylor term, which yields the estimate

$$(6.4) \quad \phi_{\|\mathbf{k}\|} = \frac{2\phi_0\sigma}{\|\mathbf{k}\|} \int_0^\infty \eta(r) \sin(2\pi\sigma\|\mathbf{k}\|r) dr \approx 4\pi\phi_0\sigma^2 \int_0^\infty r\eta(r) dr \sim \sigma^2,$$

that is, at large scales the Fourier transform of the Thomas–Fermi potential is a small constant. This, of course, is to be expected, since it is known that the effect of interatomic potentials is very limited at large scales. For the velocity and energy scaling in (5.6) and (5.7) in any bundle \mathcal{B}_{ij} at large inertial scales, this formally means that

$$(6.5) \quad \bar{U}_K \sim 1, \quad \bar{E}_K \sim \|\mathbf{k}\|^{-1}.$$

However, in practice the Thomas–Fermi potential would be unable to affect the dynamics at large scales, due to its short range (or, to put it more formally, it would not be practically possible to choose the strength of the large scale flow \bar{W}_K so that the approximate relations in (5.1) would hold).

For $\sigma\|\mathbf{k}\| \sim 1$ (that is, at small scales), the estimate above becomes invalid. Instead, one can integrate (6.3) by parts to obtain

$$(6.6) \quad \phi_{\|\mathbf{k}\|} = \frac{\phi_0}{\pi\|\mathbf{k}\|^2} \left(1 + \int_0^\infty \eta'(r) \cos(2\pi\sigma\|\mathbf{k}\|r) dr \right) \sim \|\mathbf{k}\|^{-2},$$

which means that at small scales the Fourier transform of the Thomas–Fermi potential behaves as the inverse square of the wavenumber. For the velocity and energy scaling in (5.16) and (5.17) in any bundle \mathcal{B}_{ij} at small inertial scales, this formally means that

$$(6.7) \quad \bar{U}_K \sim \|\mathbf{k}\|^{-2/3}, \quad \bar{E}_K \sim \|\mathbf{k}\|^{-5/3}.$$

Observe that the estimated energy scaling coincides with the famous Kolmogorov scaling [10, 12, 22–24, 28, 29]. Also, note that any potential of the form (6.1), whose screening function has a continuous bounded derivative – for example, the Ziegler–Biersack–Littmark potential [38] – will produce the same scaling as in (6.7).

6.2. The scaling for the electrostatic potential. From the relation in (6.6), it is easy to obtain the explicit formula for the Fourier transform of the electrostatic potential. Namely, observe that the electrostatic $1/r$ -potential can be obtained from the Thomas–Fermi potential in (7.2) by taking the limit $\sigma \rightarrow \infty$. Applying the same limit in (6.6) for $\|\mathbf{k}\| > 0$ yields

$$(6.8) \quad \lim_{\sigma \rightarrow \infty} \int_0^\infty \eta'(r) \cos(2\pi\sigma\|\mathbf{k}\|r) dr = \lim_{\omega \rightarrow \infty} \int_0^\infty \eta'(r) \cos(\omega r) dr = 0,$$

since $\eta'(r)$ is continuous and bounded, and thus its cosine Fourier transform decays to zero with increasing wavenumber. This leads to

$$(6.9) \quad \phi_{\|\mathbf{k}\|}^{el} = \frac{\phi_0^{el}}{\pi\|\mathbf{k}\|^2}.$$

As we can see, the Fourier transform for the electrostatic potential decays as $\|\mathbf{k}\|^{-2}$ throughout the whole range of Fourier wavenumbers, including the large scales. For the velocity and energy scalings in (5.6), (5.7), (5.16) and (5.17) in any bundle \mathcal{B}_{ij} , this means

$$(6.10a) \quad \bar{U}_K \sim \|\mathbf{k}\|^{-2}, \quad \bar{E}_K \sim \|\mathbf{k}\|^{-3} \quad \text{at large inertial scales,}$$

$$(6.10b) \quad \bar{U}_K \sim \|\mathbf{k}\|^{-2/3}, \quad \bar{E}_K \sim \|\mathbf{k}\|^{-5/3} \quad \text{at small inertial scales.}$$

Observe that, at small inertial scales, the energy scaling for the electrostatic potential is the same as that for the Thomas–Fermi potential in (6.7), and also coincides with the famous Kolmogorov scaling [10, 12, 22–24, 28, 29].

7. COMPARISON WITH OBSERVATIONS

Above, we estimated the scaling of the $3N \times 3N$ -dimensional matrix $\bar{\mathbf{E}}_K$, which is the Fourier transform of the full Laplace-averaged kinetic energy matrix $\bar{\mathbf{E}}(X)$, respectively. The energy matrix contains the full set of velocity moments of the second order for all particles, as functions of all their distinct locations.

Clearly, such a quantity cannot be measured in a realistic experiment or an observation. As described above in Section 3, a typical experiment or observation consists of a set of probes, which are deployed at specified locations. These probes interact with those particles which pass through their locations, and thus measure their properties. Realistically, these probes cannot distinguish between separate particles, which means that, first, the cross-particle velocity moments are difficult to capture, and, second, the same-particle velocity moments are ensemble-averaged over those particles which interact with a particular probe.

Let us assume that a probe is placed in the location \mathbf{y} in the 3-dimensional physical place, and let us presume that N_y particles (out of total N) interact with that probe during the measurement. Then, the “energetic” quantity, which can be somewhat easily captured, is the ensemble average

$$(7.1) \quad E(\mathbf{y}) = \frac{1}{N_y} \sum_{i=1}^{N_y} \text{diag}(\bar{\mathbf{E}}_i),$$

where $\bar{\mathbf{E}}_i$ are the 3×3 blocks of $\bar{\mathbf{E}}$ which correspond to the quadratic velocity self-moments of particles passing through \mathbf{y} , and lie on the main diagonal of $\bar{\mathbf{E}}$, whereas “diag” denotes the operation of extracting the main diagonal from $\bar{\mathbf{E}}_i$ and mapping it into a vector. Thus $E(\mathbf{y})$ contains the average wind energy at the location \mathbf{y} , measured in all three directions separately. The total scalar kinetic energy of the wind is, obviously, the half of the trace of $E(\mathbf{y})$.

Typically, multiple probes in different locations are used, such that the distances between measured particles are known and given by the coordinate offsets of the probes. The subsequent DFT over the set of probe coordinates \mathbf{y} reveals the scaling structure of these quantities in the bundles \mathcal{B}_{ij} in (3.6), as described above in Section 3. If, by \mathbf{k} , we denote the Fourier wavevector of the DFT in \mathbf{y} , then the corresponding Fourier transform E_k will apparently have the same bulk scaling structure as its counterpart $\bar{\mathbf{E}}_K$ in the bundles \mathcal{B}_{ij} (remember that the scaling is shared across the bundles). Therefore, from the estimates in (6.7) and (6.10), we arrive at the following relations:

- a. **The Thomas–Fermi potential.** For the Thomas–Fermi potential, E_k is estimated to scale as

$$(7.2) \quad E_k \sim \|\mathbf{k}\|^{-5/3}$$

at small inertial scales. At large inertial scales, the Thomas–Fermi potential is unlikely to have any discernible effect on dynamics.

- b. **The electrostatic potential.** For the electrostatic potential, E_k is estimated to scale as

$$(7.3a) \quad E_k \sim \|\mathbf{k}\|^{-3} \quad \text{at large inertial scales,}$$

$$(7.3b) \quad E_k \sim \|k\|^{-5/3} \quad \text{at small inertial scales.}$$

In laboratory experiments, the inverse five-thirds energy scaling at near viscous ranges, as predicted above in (7.2) and (7.3) for both the Thomas–Fermi and the electrostatic potentials, is observed rather reliably – see, for example, the recent work by Buchhave and Velte [6]. On the other hand, at larger inertial scales, the results of observations sometimes do not reveal any power scaling; for example, in [6], the energy spectrum flattens out at larger scales. This, however, does not mean that the energy spectrum becomes constant, only that there is no discernible linear trend on the log-log plot. According to our hypothesis, such an uncertain behavior at large scales is to be expected if the particles are indeed driven by the Thomas–Fermi or a qualitatively similar (for example, the Ziegler–Biersack–Littmark [38]) short-range potential, whose effect does not extend too far beyond the viscous scale.

Surprisingly, the observations of the Earth atmosphere capture a radically different behavior, where the power scaling of the energy spectrum is observed in a broad range of scales. A striking example is the work of Nastrom and Gage [27], where the observations were obtained from the Global Atmospheric Sampling Program (GASP) dataset. With the permission from the American Meteorological Society, we reproduce Figure 3 from [27] in Figure 1, which shows the energy spectra of the meridional (north–south) and zonal (east–west) winds. Both the meridional and zonal wind energy spectra exhibit the inverse cubic power scaling at large scales, and the inverse five-thirds power scaling at small scales. According to Nastrom and Gage [27], these trends appear to be universal, and largely independent on the latitude, longitude and altitude of the flow.

The observations in [27] are not consistent with the assumption that the motions at inertial scales are primarily driven via the short-range Thomas–Fermi potential, as the latter lacks any measurable ability to affect the scaling at larger scales. Yet, in [27], we see that the power scaling of the energy spectrum manifests itself up to the synoptic scales, which exceeds the effective range of the Thomas–Fermi potential by many orders of magnitude. Also, somewhat paradoxically, the observed inverse cubic spectrum at large scales and inverse five-thirds spectrum at small scales match the predictions in (7.3) for the electrostatic interaction potential, which does not have a discernible effective spatial range.

If the observed turbulent motions manifest according to our theory above, the only rational explanation for the universality of the spectra in [27] and in Figure 1 appears to be that the wind energy spectra of the atmospheric turbulence are indeed produced by the electrostatic potential. Recall that the Earth atmosphere is not electrostatically neutral – in fact, the density of ionized molecules in the air is such that the average strength of the electric field at low altitudes is about 130 volt per meter [35], so that its influence is not negligible. While the relative density of the charged particles and ionized molecules in the Earth atmosphere is relatively low (in comparison with the electrostatically neutral molecules), a possible mechanism of the statistical energy distribution is that the charged molecules collide with the electrostatically neutral molecules around them and “thermodynamically equilibrate” their energy on a much shorter time scale than the turbulent averaging time scale T . While such a hypothesis needs to be verified experimentally,

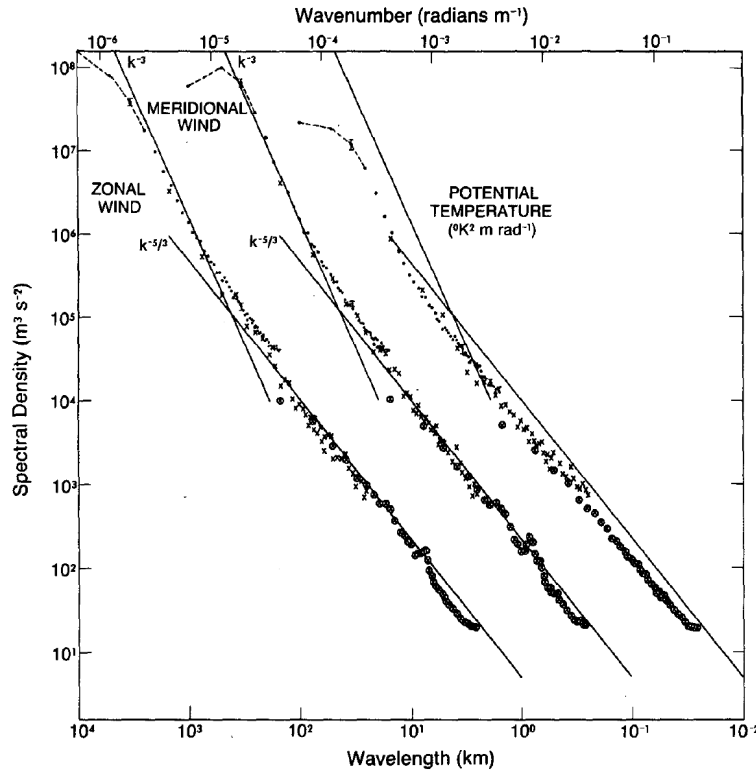


FIGURE 1. Wind energy and temperature spectra, reproduced from Fig. 3 in [27]. © American Meteorological Society. Used with permission.

it does nonetheless offer a plausible explanation for the observed power scaling of the atmospheric turbulent energy spectrum.

In addition to the meridional and zonal wind energy spectra, Nastrom and Gage [27] examined the temperature spectrum, which is also shown in Figure 1. Observe that the temperature spectrum exhibits the same scaling trends as the wind energy spectra, however, presently we do not have a straightforward explanation for this. The reason is that the temperature is, effectively, the average kinetic energy of molecules, only measured in the reference frame which moves with the average wind (and is therefore subject to the turbulent fluctuations of the wind). Therefore, the temperature is affected simultaneously by the fluctuations of the kinetic energy of the wind, as well as the fluctuations of the thermal motion in the wind reference frame, and it is not clear which fluctuations provide the dominant contribution. In addition, what is plotted in Figure 1 appears to be the square of the temperature fluctuations, since the units are indicated as “°K²” (that is, degrees Kelvin squared). Thus, we presently refrain from further comments on the displayed temperature spectrum, and will examine it in a separate work.

8. SUMMARY

In the present work, we investigate the Liouville equation for N particles, which interact via a generic potential. We find that a strong large scale flow velocity creates forcing in the inertial ranges of the energy equation via the potential coupling. This forcing

lives in the 3-dimensional bundles of the full $3N$ -dimensional coordinate space, with each bundle belonging to an unordered pair of particles. These bundles are destroyed in the course of the BBGKY formalism, so that no such forcing manifests in the Boltzmann equation, and, subsequently, in the Euler and Navier–Stokes equations. On the other hand, measurements can register the resulting flow in these bundles – effectively, these bundles are “collapsed” into the physical 3-dimensional space, where the measurement probes are located. Although an individual information in each bundle is lost during such collapse, the bulk trends, shared across all bundles, may persist.

Next, we investigate appropriately scaled time averages of solutions of the Liouville equation. In particular, we develop crude estimates for the power scaling of the energy spectrum in the inertial range, assuming that it is driven by the strong large scale flow coupled to the inertial scales via the interaction potential. The following is a summary of assumptions and simplifications we utilize above to arrive at the scaling estimates:

1. We assume that the spectrum of a physically relevant solution of the Liouville equation has three subranges: strong large scale flow, inertial range, and viscous range.
2. In the inertial range, we assume that the only measurable effect of the potential is the strong large scale velocity forcing in the energy equation.
3. We assume that the exponentially weighted time average via the Laplace transformation in Section 4 is a sufficiently close analog of a windowed time average.
4. For the time-averaged dynamics in Section 5, we make the following assumptions:
 - On the chosen averaging time scale, the flow is effectively incompressible;
 - The centered skewness moment in the inertial range can be neglected in comparison with the velocity and energy moments;
 - As the inertial range transitions into the viscous range, the time-averaged velocity rapidly decays to zero, similarly to a “cut-off”.
5. To make the spectrum decay estimates, we assume that the time-averaged solution is turbulent and its energy spectrum has power scaling, i.e. the strong large scale flow velocity has an appropriate pattern to induce turbulence in the inertial range.

Under these assumptions, we find that:

- a. In the near-viscous inertial subrange, the energy spectra are estimated to decay as the inverse five-thirds power of the Fourier wavenumber for the Thomas–Fermi interatomic potential [13,37] (or a similar one, such as the Ziegler–Biersack–Littmark potential [38]), as well as the electrostatic potential;
- b. In the large scale inertial subrange, the energy spectra are estimated to decay as an inverse cubic power of the Fourier wavenumber for the electrostatic potential, while the Thomas–Fermi interatomic potential is not expected to affect the dynamics due to its short effective range.

We compare the predictions with the measurements provided by Buchhave and Velte [6] for the turbulent flow in laboratory conditions, and by Nastrom and Gage [27] for the Earth atmosphere. The measurements in [6] appear to be consistent with the predictions for the Thomas–Fermi potential. Strikingly, the observations of Nastrom and Gage [27] indicate that, at the inertial scales, the Earth atmosphere behaves as if driven via the electrostatic potential, i.e. exhibiting the inverse five-thirds power spectrum at small

scales, and the inverse cubic spectrum at large scales. We suggest a hypothesis that, since the Earth atmosphere is not electrostatically neutral, it could indeed be the case that the atmospheric turbulent energy spectra are induced by the large scale flow coupled via the electrostatic potential.

In laboratory conditions, this hypothesis can be tested experimentally by measuring the turbulent energy spectra of a gas which is electrostatically charged to varying degrees. For a fully neutral gas, one should expect the spectra as in [6], with the inverse five-thirds scaling in near-viscous ranges due to the Thomas–Fermi potential, and an indeterminate behavior at large scales. As the electric charge of the gas increases, one should initially observe the extension of the inverse five-thirds scaling onto larger scales (where no discernible power scaling was observed for a neutral gas), and, eventually, the transition to the inverse cubic power at large scales, as in [27].

If the atmospheric turbulent motions and the related energy spectra are indeed caused by the electrostatic potential, it would be interesting to examine the behavior of large, relatively dense systems of celestial bodies (such as Saturnian rings, for example), which interact via the gravitational potential. Recall that the gravitational potential has the same form as the electrostatic potential, except for the opposite sign – while the electrostatically charged particles repel, the bodies with mass attract. This means that the same reasoning as above could likely be applied to the estimates of the kinetic energy spectra of large systems of celestial bodies.

Finally, we have to point out that the conventional Euler and Navier–Stokes equations of fluid dynamics are incapable of modeling the described effects, because the bundles, in which the latter manifest, are destroyed in the process of the BBGKY formalism. If it is indeed confirmed that the turbulent motions and the related energy spectra appear as described in the present work, the conventional equations of the fluid dynamics will likely have to be appropriately modified to extend their applicability onto turbulent motions in the inertial ranges.

APPENDIX A. THE STRUCTURE OF THE POTENTIAL

Recalling (2.4), for the Fourier transform $\Phi_{\mathbf{K}}$ in (2.14) we write

$$(A.1) \quad \Phi_{\mathbf{K}} = \int_{\mathbb{R}^{3N}} \Phi(\mathbf{X}) e^{-i\mathbf{K}\cdot\mathbf{X}} d\mathbf{X} = \sum_{i=1}^{N-1} \sum_{j=i+1}^N \int_{\mathbb{R}^{3N}} e^{-i\mathbf{K}\cdot\mathbf{X}} \phi(\|\mathbf{x}_i - \mathbf{x}_j\|) d\mathbf{X}.$$

For each individual integral in the sum, we can write

$$(A.2) \quad \int_{\mathbb{R}^{3N}} e^{-i\mathbf{K}\cdot\mathbf{X}} \phi(\|\mathbf{x}_i - \mathbf{x}_j\|) d\mathbf{X} = \prod_{\substack{m=1 \\ m \neq i,j}}^N \delta(\mathbf{k}_m) \int_{\mathbb{R}^6} e^{-i(\mathbf{k}_i \cdot \mathbf{x}_i + \mathbf{k}_j \cdot \mathbf{x}_j)} \phi(\|\mathbf{x}_i - \mathbf{x}_j\|) d\mathbf{x}_i d\mathbf{x}_j = \\ = \delta(\mathbf{k}_i + \mathbf{k}_j) \prod_{\substack{m=1 \\ m \neq i,j}}^N \delta(\mathbf{k}_m) \int_{\mathbb{R}^3} e^{-i\hat{\mathbf{k}}_i \cdot \mathbf{y}} \phi(\|\mathbf{y}\|) d\mathbf{y}.$$

For the remaining 3D-integral, we switch to the spherical coordinate system (r, α, β) , whose polar axis is aligned with \mathbf{k} , such that $\mathbf{k} \cdot \mathbf{y} = \|\mathbf{k}\|r \cos \beta$. This yields

$$(A.3) \quad \int_{\mathbb{R}^3} e^{-\hat{\mathbf{i}}\mathbf{k} \cdot \mathbf{y}} \phi(\|\mathbf{y}\|) d\mathbf{y} = \int_0^\pi \int_0^{2\pi} \int_0^\infty e^{-\hat{\mathbf{i}}\|\mathbf{k}\|r \cos \beta} \phi(r) r^2 \sin \beta dr d\alpha d\beta.$$

The integral over the angles alone yields

$$(A.4) \quad \int_0^\pi \int_0^{2\pi} e^{-\hat{\mathbf{i}}\|\mathbf{k}\|r \cos \beta} \sin \beta d\alpha d\beta = \frac{2}{\|\mathbf{k}\|r} \sin(2\pi\|\mathbf{k}\|r),$$

which leads to

$$(A.5) \quad \int_{\mathbb{R}^3} e^{-\hat{\mathbf{i}}\mathbf{k} \cdot \mathbf{y}} \phi(\|\mathbf{y}\|) d\mathbf{y} = \frac{2}{\|\mathbf{k}\|} \int_0^\infty r \phi(r) \sin(2\pi\|\mathbf{k}\|r) dr.$$

At this point, denoting $\phi_{\|\mathbf{k}\|}$ as in (3.4), and assembling the pieces together, we arrive at (3.3).

APPENDIX B. THE AVERAGING LIMIT OF THE LAPLACE TRANSFORMATION

Here we follow the proof given in [16, Section 2.1]. Let $G(T)$ denote the T -window average of F :

$$(B.1) \quad G(T) = \frac{1}{T} \int_0^T F(t) dt.$$

Assuming that the limit of $G(T)$ as $T \rightarrow \infty$ exists, the Final Value theorem states that

$$(B.2) \quad \lim_{T \rightarrow \infty} G(T) = \lim_{s \rightarrow 0} s \mathcal{L}\{G\}(s).$$

We are going to show that, in addition to the above identity,

$$(B.3) \quad \lim_{s \rightarrow 0} s \mathcal{L}\{G\}(s) = \lim_{s \rightarrow 0} s \mathcal{L}\{F\}(s).$$

First, observe that

$$(B.4) \quad \mathcal{L}\{G\}(s) = \int_0^\infty e^{-st} G(t) dt = \int_0^\infty e^{-st} \left(\frac{1}{t} \int_0^t F(\tau) d\tau \right) dt.$$

At the same time, note that

$$(B.5) \quad \frac{e^{-st}}{t} = \int_s^\infty e^{-pt} dp,$$

and, therefore,

$$(B.6) \quad \begin{aligned} \mathcal{L}\{G\}(s) &= \int_0^\infty \left(\int_s^\infty e^{-pt} dp \right) \left(\int_0^t F(\tau) d\tau \right) dt = \int_0^\infty dt \int_s^\infty dp e^{-pt} \int_0^t F(\tau) d\tau = \\ &= \int_s^\infty dp \int_0^\infty dt e^{-pt} \int_0^t F(\tau) d\tau = \int_s^\infty \mathcal{L} \left\{ \int_0^t F(\tau) d\tau \right\} (p) dp. \end{aligned}$$

Above, Fubini's theorem was used to interchange the order of integration in dt and dp , given that all integrands are nonnegative (as F is a probability density), and under the

further assumption that the resulting integral is finite. To verify the latter, observe that, from the derivative formula for the Laplace transformation we know that

$$(B.7) \quad \mathcal{L}\{F\}(p) = p\mathcal{L}\left\{\int_0^t F(\tau)d\tau\right\}(p), \quad \text{or} \quad \mathcal{L}\left\{\int_0^t F(\tau)d\tau\right\}(p) = \frac{1}{p}\mathcal{L}\{F\}(p).$$

Assuming that F is bounded, its Laplace image is estimated as

$$(B.8) \quad \mathcal{L}\{F\}(p) \sim \frac{1}{p}, \quad \text{and, therefore,} \quad \frac{1}{p}\mathcal{L}\{F\}(p) \sim \frac{1}{p^2}.$$

Thus, the integral of the latter expression from s to ∞ is finite as long as $s > 0$, which means that the use of Fubini's theorem above is justified. Combining (B.6) and (B.7), we arrive at

$$(B.9) \quad \mathcal{L}\{G\}(s) = \int_s^\infty \frac{1}{p}\mathcal{L}\{F\}(p)dp, \quad \text{or} \quad s\mathcal{L}\{G\}(s) = s \int_s^\infty \frac{1}{p}\mathcal{L}\{F\}(p)dp.$$

The limit of the latter expression as $s \rightarrow 0$ can be computed via L'Hôpital's "0/0" rule:

$$(B.10) \quad \lim_{s \rightarrow 0} s\mathcal{L}\{G\}(s) = \lim_{s \rightarrow 0} \frac{\int_s^\infty \frac{1}{p}\mathcal{L}\{F\}(p)dp}{1/s} = \lim_{s \rightarrow 0} \frac{-\frac{1}{s}\mathcal{L}\{F\}(s)}{-1/s^2} = \lim_{s \rightarrow 0} s\mathcal{L}\{F\}(s).$$

Finally, replacing $s = T^{-1}$ in the right-hand side and recalling (4.5) yields (4.3).

Acknowledgment. The author thanks the American Meteorological Society for granting the permission to reproduce Figure 3 from the article by Nastrom and Gage [27]. This work was supported by the Simons Foundation grant #636144.

REFERENCES

- [1] R.V. Abramov. The random gas of hard spheres. *J.*, 2(2):162–205, 2019.
- [2] N.N. Bogoliubov. Kinetic equations. *J. Exp. Theor. Phys.*, 16(8):691–702, 1946.
- [3] L. Boltzmann. Weitere Studien über das Wärmegleichgewicht unter Gasmolekülen. *Sitz.-Ber. Kais. Akad. Wiss. (II)*, 66:275–370, 1872.
- [4] M. Born and H.S. Green. A general kinetic theory of liquids I: The molecular distribution functions. *Proc. Roy. Soc. A*, 188:10–18, 1946.
- [5] J. Boussinesq. Essai sur la théorie des eaux courantes. *Mémoires présentés par divers savants à l'Académie des Sciences*, XXIII(1):1–680, 1877.
- [6] P. Buchhave and C.M. Velte. Measurement of turbulent spatial structure and kinetic energy spectrum by exact temporal-to-spatial mapping. *Phys. Fluids*, 29(8):085109, 2017.
- [7] R.A. Buckingham. The classical equation of state of gaseous helium, neon and argon. *Proc. R. Soc. Lond. A*, 168:264–283, 1938.
- [8] C. Cercignani. *Theory and Application of the Boltzmann Equation*. Elsevier Science, New York, 1975.
- [9] C. Cercignani, R. Illner, and M. Pulvirenti. The mathematical theory of dilute gases. In *Applied Mathematical Sciences*, volume 106. Springer-Verlag, 1994.
- [10] S. Chandrasekhar. On Heisenberg's elementary theory of turbulence. *Proc. Roy. Soc.*, 200:20–33, 1949.
- [11] S. Chapman and T.G. Cowling. *The Mathematical Theory of Non-Uniform Gases*. Cambridge Mathematical Library. Cambridge University Press, 3rd edition, 1991.
- [12] S. Corrsin. On the spectrum of isotropic temperature fluctuations in an isotropic turbulence. *J. Appl. Phys.*, 22(4):469–473, 1951.
- [13] E. Fermi. A statistical method for determining some properties of the atom. *Rend. Accad. Naz. Lincei*, 6:602–607, 1927.

- [14] I. Gallagher, L. Saint-Raymond, and B. Texier. *From Newton to Boltzmann: Hard Spheres and Short-Range Potentials*. European Mathematical Society, Zürich, Switzerland, 2014.
- [15] I.I. Gikhman and A.V. Skorokhod. *Introduction to the Theory of Random Processes*. Courier Dover Publications, 1969.
- [16] E. Gluskin and S. Miller. On the recovery of the time average of continuous and discrete time functions from their Laplace and z -transforms. Preprint available at <https://arxiv.org/abs/1109.3356>, 2012.
- [17] F. Golse. *The Boltzmann Equation and its Hydrodynamic Limits*, volume 2 of *Handbook of Differential Equations: Evolutionary Equations*, chapter 3, pages 159–301. Elsevier, 2005.
- [18] H. Grad. On the kinetic theory of rarefied gases. *Comm. Pure Appl. Math.*, 2(4):331–407, 1949.
- [19] J.O. Hirschfelder, C.F. Curtiss, and R.B. Bird. *The Molecular Theory of Gases and Liquids*. Wiley, 1964.
- [20] J.G. Kirkwood. The statistical mechanical theory of transport processes I: General theory. *J. Chem. Phys.*, 14:180–201, 1946.
- [21] S. Kobayashi, T. Matsukuma, S. Nagai, and K. Umeda. Accurate value of the initial slope of the ordinary TF function. *J. Phys. Soc. Jpn.*, 10:759–762, 1955.
- [22] A.N. Kolmogorov. Decay of isotropic turbulence in an incompressible viscous fluid. *Dokl. Akad. Nauk SSSR*, 31:538–541, 1941.
- [23] A.N. Kolmogorov. Energy dissipation in locally isotropic turbulence. *Dokl. Akad. Nauk SSSR*, 32:19–21, 1941.
- [24] A.N. Kolmogorov. Local structure of turbulence in an incompressible fluid at very high Reynolds numbers. *Dokl. Akad. Nauk SSSR*, 30:299–303, 1941.
- [25] J.E. Lennard-Jones. On the determination of molecular fields. – II. From the equation of state of a gas. *Proc. R. Soc. Lond. A*, 106(738):463–477, 1924.
- [26] C.D. Levermore. Moment closure hierarchies for kinetic theories. *J. Stat. Phys.*, 83:1021–1065, 1996.
- [27] G.D. Nastrom and K.S. Gage. A climatology of atmospheric wavenumber spectra of wind and temperature observed by commercial aircraft. *J. Atmos. Sci.*, 42(9):950–960, 1985.
- [28] A.M. Obukhov. On the distribution of energy in the spectrum of a turbulent flow. *Izv. Akad. Nauk SSSR Ser. Geogr. Geofiz.*, 5:453–466, 1941.
- [29] A.M. Obukhov. Structure of the temperature field in turbulent flow. *Izv. Akad. Nauk SSSR Ser. Geogr. Geofiz.*, 13:58–69, 1949.
- [30] A.M. Obukhov. Some specific features of atmospheric turbulence. *J. Geophys. Res.*, 67(8):3011–3014, 1962.
- [31] B. Øksendal. *Stochastic Differential Equations: An Introduction with Applications*. Universitext. Springer, 6th edition, 2010.
- [32] O. Reynolds. An experimental investigation of the circumstances which determine whether the motion of water shall be direct or sinuous, and of the law of resistance in parallel channels. *Proc. R. Soc. Lond.*, 35(224–226):84–99, 1883.
- [33] O. Reynolds. On the dynamical theory of incompressible viscous fluids and the determination of the criterion. *Phil. Trans. Roy. Soc. A*, 186:123–164, 1895.
- [34] H. Risken. *The Fokker-Planck Equation*. Springer-Verlag, New York, 2nd edition, 1989.
- [35] R.C. Sagalyn, H.K. Burke, and D.R. Fitzgerald. Atmospheric electricity. In A.S. Jursa, editor, *Handbook of Geophysics and the Space Environment*, chapter 20, pages 1–37. National Technical Information Service, Springfield, VA, 1985.
- [36] A. Sommerfeld. Asymptotic integration of the Thomas–Fermi differential equation. *Rend. Accad. Naz. Lincei*, 15:788–792, 1932.
- [37] L.H. Thomas. The calculation of atomic fields. *Proc. Camb. Phil. Soc.*, 23(5):542–548, 1927.
- [38] J.F. Ziegler, J.P. Biersack, and U. Littmark. *The Stopping and Range of Ions in Solids*, volume 1 of *Stopping and Ranges of Ions in Matter*. Pergamon, 1985.